RESEARCH ARTICLE

Design of the Stable Homogeneous Magnetic Field Calibration Device Generated by the Circular Coils

SHAO SYUAN SYU[1]**, MANCHALA GOPALA KRISHNA**[2]**,
ROSHNI YADAV**[1]**, (Graduate Student Member, IEEE),
AND KO-WEI LIN**[1]**, (Senior Member, IEEE)**
[1]Department of Materials Science and Engineering, National Chung Hsing University, Taichung 402, Taiwan
[2]Magnetoelectric Research and Development Laboratory, Mobilsens Technologies, Taichung 407, Taiwan

Corresponding author: Ko-Wei Lin (kwlin@dragon.nchu.edu.tw)

ABSTRACT This research relates to manufacturing stable homogeneous magnetic field strength generating equipment. It refers to the stable homogeneous magnetic field device's design method in the theoretical, finite element, and experimental methods, which is beneficial for generating high homogeneous magnetic field strength. The circular coils produce the uniform magnetic field strength for a given number of winding turns and distance between the pair of coils. The number of turns of each coil and gauge of the wire for the winding was adjusted by theoretical calculations. The coil's current carrying capacity determines the high magnetic field strength. The uniformity of the magnetic field is based on the size and current density of the coils. This paper emphasizes the theoretical formula to calculate a couple of values and then apply a finite element method for the verification. The finite element method values are compared with the theoretical values for proofreading. The different current values are applied, showing the increase in the magnetic field strength from low to high current values. The coils are made using the same theory and finite element method parameters. The experimental values are similar to the simulation values, with a maximum error percentage of 3.08 %. The magnetic field homogeneity distribution at the middle of the two coils is less than 1% of error. The magnetic flux density in the center of the two coils is measured using a high-precision Gauss meter.

INDEX TERMS Circular coils, electromagnet, homogeneous magnetic field, Helmholtz coils.

I. INTRODUCTION

In present days, magnetic field generation is used for various medical, industrial, and aerospace applications. Stable homogeneous magnetic fields are in high demand due to application requirements. There are a variety of applications in numerous subject fields that need the creation of a homogeneous magnetic field, such as microfluidic applications [1], active shielding [2], electromagnetic compatibility [3], navigation systems [4], and magnetic torque sensors for steering system [5]. The Earth's magnetic field can be utilized to locate and control satellites [6], [7], [8]. The cathode ray tubes are used in many applications such as televisions, computer

The associate editor coordinating the review of this manuscript and approving it for publication was Bo Pu.

monitors, and oscilloscopes, where the coils are used for the magnetic deflection of electrons in cathode ray tubes [9], [10], [11].

The system was used to generate a uniform magnetic field, depending on the coil's geometrical shape [12]. Coils are very useful as small magnets and generate a wide range of magnetic fields in unique shapes like arcs and squares.

Generally, coils are available in various shapes and sizes, including circular, solenoidal, and spherical coils. Unlike the other coils, the circular Helmholtz coil produces a homogeneous magnetic field [13]. The circular coils are used in MRI machines for magnetic field strength. Here, the coils act as receivers for the human body's radio frequency signals and transfer them to the computer for images [14], [15], [16], [17]. The two coils are arranged at the required distance, and

the current source is applied as per the electrical parameters. Thus, it produces a stable homogeneous magnetic field strength [18].

This research aims to provide a design methodology for a stable homogeneous magnetic field generating device. The magnetic field's variable characteristics are caused by different current magnitudes generating an adjustable and stable magnetic field to overcome the permanent magnet problems. Permanent magnets have a fixed magnetic field strength and are not easy to use, so this is the reason for designing a stable homogeneous magnetic field generating device. In the present research, the first method is theory calculations used to derive the theoretical formula and related setting parameters into a theoretical formula to calculate one set of magnetic field strength (H) values. Each set contains eight values with the current variation (I = 0.25 A to I = 2.0 A). The second method is simulation calculations. The Finite Element Method (FEM) is used in these simulation calculations [19].

The simulation work is done by the magnetic simulation software of JMAG [20], [21], [22], [23], [24]. In order to do the simulation as a first step, the Computer-Aided Design (CAD) of the calibration device transfers to the simulation software as a step file. The input parameters were given corresponding to the theoretical method and simulated a set of values. The third method implements the second method, which is experimental measurement. We made the two coils using the same parameters used in the simulations. A set of magnetic field strength experimental values were measured with the probe. The high precision probe was used to measure the experimental values [25], [26], [27].

The Gauss meter is Magnet-Physik (MPS) FH 54. This is high-accuracy equipment, easy handling with a multitude of functions. The entire range is from 0 - 3 Tesla (T). The basic accuracy of this probe is 0.3%, and the precision is 0.2%. The accuracy of the Gauss meter probe will affect the measurement values. The Gauss meter measurement probe's accuracy is based on the permanent magnet because the permanent magnet's magnetic field strength is relatively stable and reliable. So when it is necessary to calibrate the measurement probes at different magnetic field strength values, the different permanent magnets are required to see the accuracy of the probe.

II. DESIGN METHOD OF THE CALIBRATION SYSTEM

The magnetic flux density should be stable and uniform for the calibration of the Gauss meters. A Helmholtz Coil concept is used in the design process of a stable homogeneous magnetic field generating device. This condition is useful to get high uniformity in the central of the two coils. Its structure includes a pair of ring-shaped conductor coils. Each conductor coil carries a current in the same direction. As shown in Fig. 1(a), the two coils are arranged parallel and decided to give the current in series connection. The distance between the two coils was arranged as 5 mm. The simple derivative model of the stable homogeneous calibration device was designed in Fig. 1(b) from the Biot-Savart law concept.
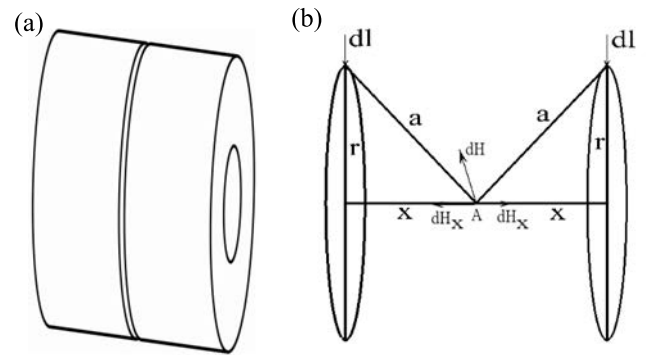

FIGURE 1. (a) CAD model of the calibration device. (b) Simple derivative model of the stable homogeneous calibration device.

A. STABLE HOMOGENEOUS COILS SIMPLE DERIVATION

This section finds the conceptual foundation for the circular coil's development. The Biot-Savart law can calculate the magnetic field's strength surrounding a current-carrying conductor wire. A current-carrying in a circular wire of radius r generates the magnetic field dH at point A as shown in Fig. 1(b). The field's axial component is:

$$dH = \frac{I}{4\pi} \frac{dl}{a^2} \sin\alpha \qquad (1)$$

While $a = \sqrt{r^2 + x^2}$ and

$$sin\alpha = \frac{r}{\sqrt{r^2 + x^2}} \qquad (2)$$

The magnetic field H at the distance X from the axis is

$$H = \int dh = \frac{1}{2\pi r^2} \sin\alpha \int dl = \frac{1}{2} I \frac{r^2}{\left(\sqrt{r^2 + x^2}\right)^3} \qquad (3)$$

According to the preceding equation, the magnetic field created by the circular coil is

$$H = \frac{nIr^2}{2} \left[r^2 + \left(\frac{L}{2} + x\right)^2 \right]^{-3/2} \qquad (4)$$

where n is the number of turns in the coil, r is the coil's radius, and L is the single coil's length. The magnetic field strength between the two coils, according to the equation, is [28].

$$H = \frac{nIr^2}{2} \left\{ \left[r^2 + \left(\frac{L}{2} + x\right)^2 \right] \right\}^{-3/2}$$
$$+ \left\{ \left[r^2 + \left(\frac{L}{2} - x\right)^2 \right] \right\}^{-3/2} \qquad (5)$$

B. STRUCTURE OF THE CALIBRATION DEVICE

The flow charts shown in Fig. 2 and Fig. 3 represent the simple visual representation of the step-by-step process. This research was solved in three methods: theoretical, finite element method, and experimental, as shown in the flow charts. Flow charts are divided into two parts:
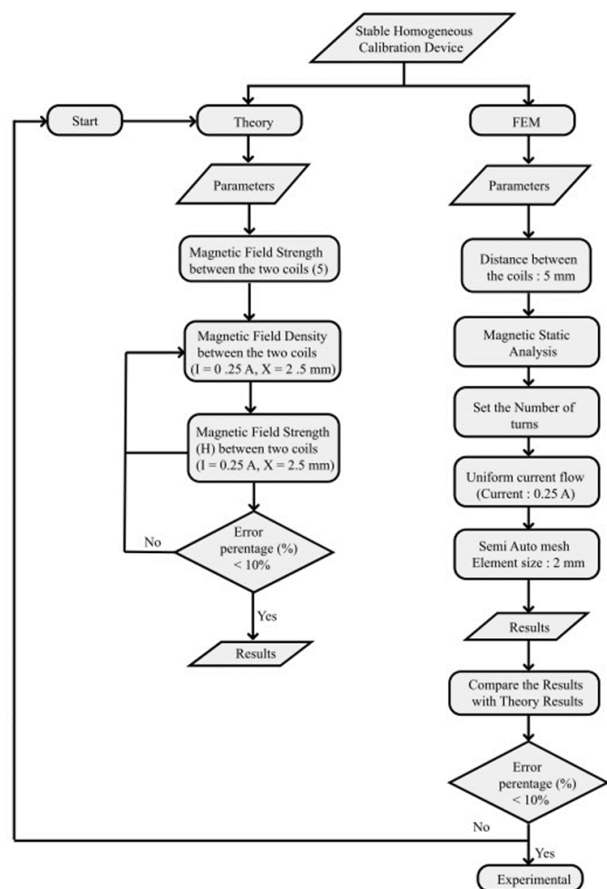
FIGURE 2. M odel flow chart for the steps of theory and FEM.

FIGURE 3. Ideal flow chart for the steps of the experimental process.

1) MODEL FLOW CHART FOR THE STEPS OF THEORY AND FEM

The model flow chart, as shown in Fig. 2, contain the two design methods, i.e., theory and FEM. At each design method, arrow marks reveal the steps of the designing process. The magnetic field strength (H) target value is fixed with the required parameters for designing a stable homogeneous calibration device, as shown in Fig. 2. The parameters are coil radius, coil length, the total number of coil turns, wire radius, the distance between the coils, and the current size. The target value is obtained by calculating (5) with the help of the parameters.

We have calculated magnetic field strength values by increasing the Ampere (A) value. The value is from $I = 0.25$ A to $I = 2.0$ A, and 0.25 A is the fixed interval of the current as a calculation step. The model flow chart's FEM method is for the proofreading of the theory method. The magnetic field strength simulations were done by the magnetic simulation software, which includes the parameters such as the number of turns, the wire radius, the coil's material, and the distance between the two coils. Using the current, $I = 0.25$ A to $I = 2.0$ A, every step size as 0.25 A as an analog step simulates a couple of values. If the finite element method value's error percentage (%) with the target value is less than
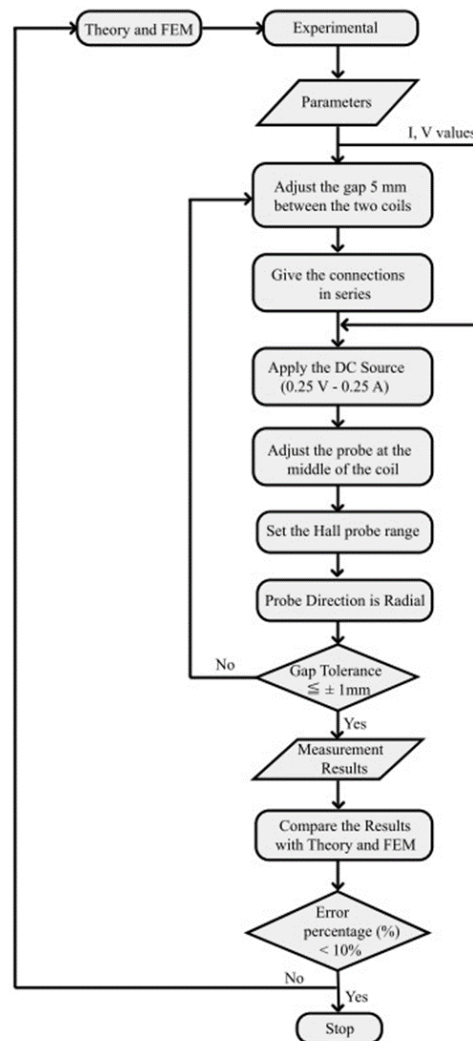
10%, the value is accepted and the ideal method is used. If not, return to the theoretical method, recheck the coil parameters, and repeat the procedure.

2) IDEAL FLOW CHART FOR THE STEPS OF THE EXPERIMENTAL PROCESS

As shown in Fig. 3, an ideal flow chart indicates the direction of the research work's progression and implements the experimental values. The two coils were manufactured according to the parameters of the coil, which are used in the calculation of theory and simulation. The two coils were arranged for the measurement by adjusting the air gap of 5 mm between them. A couple of values were measured by increasing the D.C. current and voltage. Here follows the same analog measuring process of Theory and FEM. The results were compared to the model's flow chart theory and FEM results. If the error percentage value is less than 10% of the target value, the prototype is accepted. If the error percentage is greater

than 10%, return to the experimental steps of gap adjusting between the two coils and repeat the procedure. If the same error percentage is observed, repeat the initial theoretical steps, double-check the parameters and calculations, and then repeat the process steps, simulating a new set of finite element method values.

3) BASIC PARAMETERS OF CIRCULAR COIL AND COIL FABRICATION

The coil parameters were considered for the theory, simulations, and experiments, as shown in Table 1. In addition, all the parameters are used for the magnetic static analysis, especially in the D.C. field.

TABLE 1. Parameters and operating conditions of the coil.

Parameter	Units	Value
number of turns	n	1050
length	mm	80
outer diameter	mm	125
inner diameter	mm	50
air gap	mm	5
current	A	0.25 – 2.0
operating voltage	V	1.5 – 12
device resistance	Ohms	5.5 – 6.5
device power	Watt	24
temperature	° C	25.00

Coils usually consist of several turns of wire wounds. Coil winding is the most important factor which affects our target magnetic flux density. A winding machine was used to wind the coils. The similar and firm winding in the circular coils ensures an optimum field. The conventional circular coils are relatively easy to wind, and they have fewer chances of deviation from the design area compared with square coils. The two circular coils were made for this research work. Each coil winding was designed with 1050 turns, an inner diameter of 50 mm, an outer diameter of 125 mm, and a length of 80 mm. The copper was used as a conducting material for the coil. The conductor wire cross-section was selected in a round shape, and the wire insulation thickness was 0.10 mm. Theoretically, copper is a superconducting material. It could be suitable for the coils, but every superconducting material has limited current density and magnetic field strength. The electrical use of copper wire was determined with the help of the American Wire Gauge. Each layer of the coil's outer diameter was measured and adjusted to be existing with the selected dimensions. Ensure the precise position of copper wire winding to avoid the excess diameter of the coil after winding. The number of layers and the number of turns per layer wound on the surface of the particular type of plastic bobbin has been installed in the winding machine. The bobbin could be easily removed after the winding of the coils procedure. The coil's surface was wrapped with 0.5 mm thick tape as insulation. One of the coil's essential factors in maintaining the resistance (R) as small as possible is to reduce the power dissipation.

III. RESULTS

A. THEORY CALCULATIONS

Homogeneous magnetic field strengths are required to calibrate the field strength meters with hall probes or determine the area turns of measuring coils. Generally, the magnetic field strength depends on the position and distance from the surfaces of the coil. The theoretical calculations contain the conceptual base to develop the circular coils for the Biot-Savart law's calibration device. The Biot-Savart law helps to calculate the magnetic field strength (H) at selected point (A) distanced by 'X' from the elementary part dl with a current 'I' as shown in Fig. 1(b). Here X is the distance of a coil from the centre point between the two coils. Our objective is to find a magnetic flux density (B) between the two identical dimensional circular coils which are with the outer radius (a), inner radius (b), and length (z), as shown in Fig. 4, with the various current values from I = 0.25 A to I = 2.0 A. The distance between the two coils was arranged as 5 mm because we observed this is the suitable distance for our target value after calculating the several distances between the two coils. The centre point is at 2.5 mm, so the X – value is 2.5 mm.
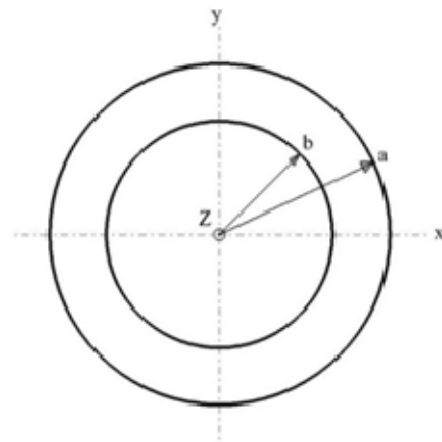

FIGURE 4. Geometry of the coils for the target field.

Generally, the magnetic field strength is generated by passing the current through coil winding turns arranged on a circular surface. Therefore, as a first step, we calculated the number of turns of the coils with the help of the target magnetic field strength value, coil parameters, and current values using the magnetic field strength (5). The coil parameters were adjusted with our device requirements. Next, the set of magnetic flux density values was calculated by using the parameters circular coils, current (I), the distance between the two coils, and the number of turns (N) with the help of (5) in different currents, as shown in Table 4. The maximum flux density is 252 Gauss (G) at the 2.0 A current. This value is near our target value with an error percentage of 0.7%. Fig.5 shows the graphical view of magnetic flux density vs. current, the increasing magnetic flux density as the current increases, and the high linearity curve.
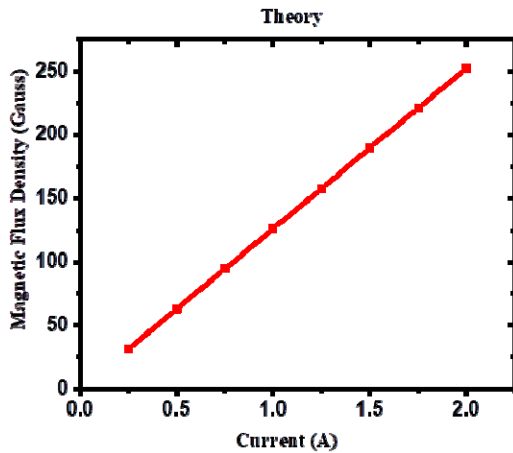
FIGURE 5. Magnetic flux density vs. current in theory.

B. FEM CALCULATIONS

These days, computer simulations have played an essential role in developing new devices. The simulation was implemented with the support of FEM, here performed three-dimensional numerical simulations. Simulations allow concepts and ideas to be verified and understood more easily. This type of research simulation has been reported in previous works [29], [30], [31], [32], [33], [34], [35]. This method's main objective is to ensure the theoretical method and observe the effects of magnetic field strength, magnetic flux lines, magnetic flux density, and magnetic vector plots. The simulation was done with the magnetic static analysis environment because of its simplicity and relevant results. Typically meshing is a significant step in the simulation analysis, and the number of nodes and elements depends on the geometrical dimensions of the coils. The semi-auto mesh function was selected in the meshing process, improving accuracy while maintaining speed. The geometrical and electrical parameters considered to conduct a simulation are shown in Table 1. The following results were obtained after the mesh and solving the processes, and the results are represented in a three-dimensional view, as shown in Fig. 6. Those are magnetic field strength ((Fig. 6(a)), magnetic field strength flux lines ((Fig. 6(b)). The magnetic field strength flux lines measure the total magnetic field strength, and it is a useful tool for describing the effects of the magnetic force on a given area. The magnetic flux density ((Fig. 6(c)) arises due to the force acting per unit current and unit length on a current-carrying conductor. The magnetic field strength vector plot ((Fig. 6(d)) represents the specified magnitude and direction of magnetic field strength at any point of the circular coils. The stable and homogeneous magnetic field strength values were observed from the simulation results. Magnetic flux density values were measured at an equal distance between the two coils with the particular sectional area, as shown in Table 4 simulation values. These simulation values are similar to the theoretical values. Table 5 displays the observed error
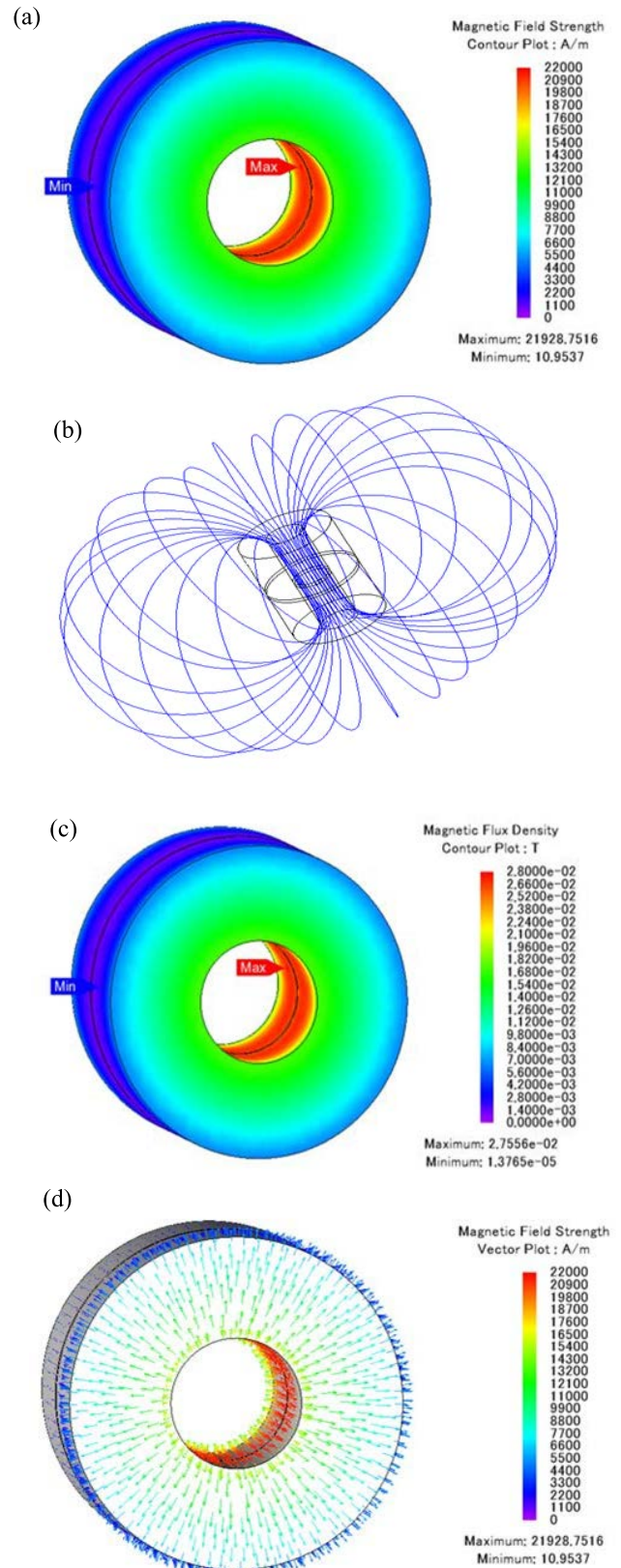

FIGURE 6. Simulation diagrams of the coils: (a) Magnetic Field Strength (A/m), (b) Magnetic field strength flux lines, (c) Magnetic flux density (T), and (d) Magnetic field strength vector plot (A/m).

percentage of the simulation values when compared to the theoretical values.

C. EXPERIMENTAL MEASUREMENTS

The complete experimental setup of the stable homogeneous device circular coils is arranged with a 5 mm air gap between the two coils, as shown in Fig. 7. The circular coil resistance (R) depend on the coil's dimensions. In this research work, we have used the coil wire diameter d = 1.5 mm with an electrical resistance of R = 5.5 Ω to R = 6.5 Ω. The DC power supply was used as a current source, and the two coils are connected in a series circuit, where each coil contains a number of conductive turns and carries a current. The direction of the magnetic field depends on the current direction, and the direction does not affect the value of flux density. The magnetic flux density (B) mainly depends on the number of turns of the coil and the operating current. The MPS FH 54 Gauss meter is used to find the magnetic field strength. Set the measurement range of a measuring probe 0-3 T before measuring the magnetic flux density, choosing the zero probe in the Gauss meter, and waiting a few seconds for the probe value to get stable and avoiding the earth magnetic field strength value. This method is very efficient and helpful in measuring the values from an ultra-low magnetic flux density. The measuring probe is inserted between the two coils in the radial direction, and the tip of the measuring probe falls within or near 2.5 mm of the line connecting the two coil's center lines. It passes the current to the two coils, with the current I = 0.25 A to I = 2.0 A as the interval, each 0.25 A is the measurement level, the voltage value is V = 1.5 V to V = 12 V, and the measurement can get a set of practical values. The obtained experimental values are mentioned in Table 4. Due to the high precision Gaussmeter, only one value after the decimal point is observed.
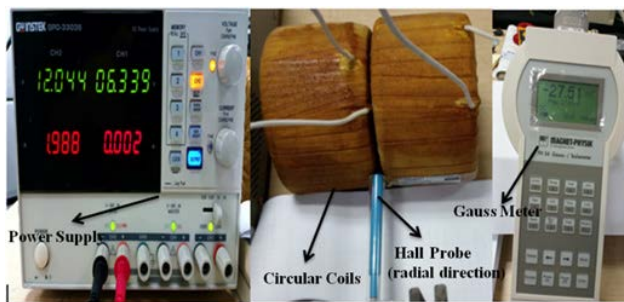

FIGURE 7. Schematic diagram of the experimental setup.

In order to validate the theory and simulation methods, experimental measurements were performed. Fig. 8 shows the graphical view of the magnetic flux density of the experimental method and FEM in Gauss. This graphical view also shows a similar linearity curve to the theory and FEM curve. The graphical view shows that magnetic flux density increases by increasing the current. The magnetic flux density values were measured between the two circular coils within the 1 mm radius circular section area at different angles at
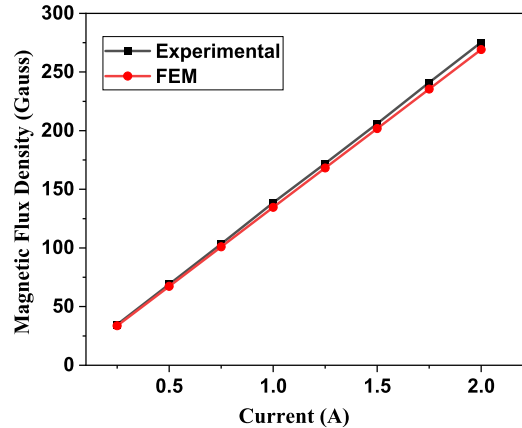

FIGURE 8. Magnetic flux density vs. current in FEM and experimental.

each current value. However, all angles contain similar magnetic flux density values, so we have considered the average value among those values shown in Table 4.

D. MAGNETIC FIELD HOMOGENEITY

The magnetic field homogeneity refers to a uniformity of a magnetic field at the center part of the calibration device. Generally, the magnetic field homogeneity is based on the number of winding turns of the coil, inner and outer diameters of the coils, and coil positions. The magnetic field homogeneity was evaluated by measuring the magnetic flux density in different positions at the 50 mm circular area diameter in the center of the two coils. However, the magnetic flux density was measured at five positions, such as the X-axis direction (1, 2, 3 positions) and Y-axis direction (4, 5 positions), as shown in Fig. 9. The magnetic field homogeneity was evaluated by randomly selected magnetic flux density values from 35 G to 275 G. These values are denoted as standard values. The measured standard values of magnetic flux densities at different positions are mentioned in Table 2.
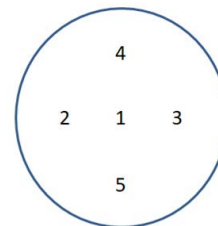
FIGURE 9. Positions to measure homogeneity.

The magnetic field distributions at standard values of 35 G, 100 G, 200 G, 250 G, and 275 G are shown in Fig. 10. The magnetic field homogeneity curves in all positions are approximately straight lines at each standard value. This indicate the calibration device has a stable homogeneous magnetic field.

In order to find the error percentage of homogeneity distribution in the middle of the device. Then, the error percentage

TABLE 2. Magnetic flux density at different positions.

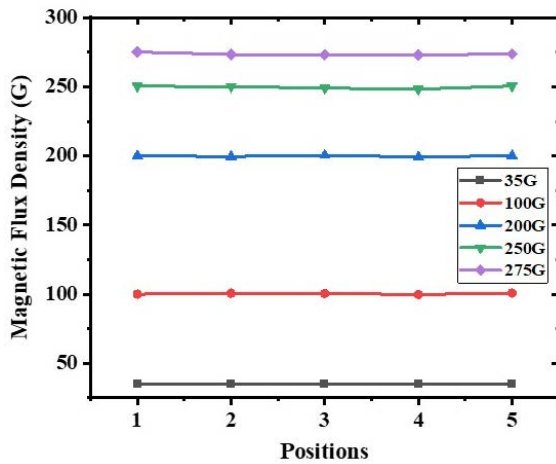| S.No	Positions	Standard value 35.0 G	Standard value 100.0 G	Standard value 200.0 G	Standard value 250.0 G	Standard value 275.0 G
1	1	35.0	100.0	200.0	250.4	275.2
2	2	34.8	100.6	199.6	250.2	273.4
3	3	34.7	100.5	200.5	249.0	273.2
4	4	34.8	99.8	199.2	248.3	273.0
5	5	34.7	100.8	200.2	250.6	273.8

FIGURE 10. Magnetic field homogeneity at different positions.

was measured at standard value (S.V) with the help of measurement value (M.V) in every position.

The position error percentage values are calculated using a standard and position values. Then, the average of position error percentage values is calculated from all position error percentage values at every standard value, as shown in Table 3.

TABLE 3. Average of standard value and error percentage.

S.No	Standard value (Gauss)	Average of Standard value (Gauss)	Average of Positions error percentage (%)
1	35	34.80	0.71
2	100	100.34	0.53
3	200	199.90	0.45
4	250	249.70	0.37
5	275	273.72	0.27

Fig. 11 shows the homogeneity error percentage of the calibration device. As mentioned in Table 3, the homogeneity curve was obtained from standard values and the average positions error percentage. The higher homogeneity error percentage is obtained at the 35 G standard value and the lower homogeneity error percentage is obtained at the 275 G standard value, as shown in Table 3. As a result, the homogeneity curve decreases from 0.71% to 0.27%, as shown in Fig. 11. The lower homogeneity error percentage occurs at
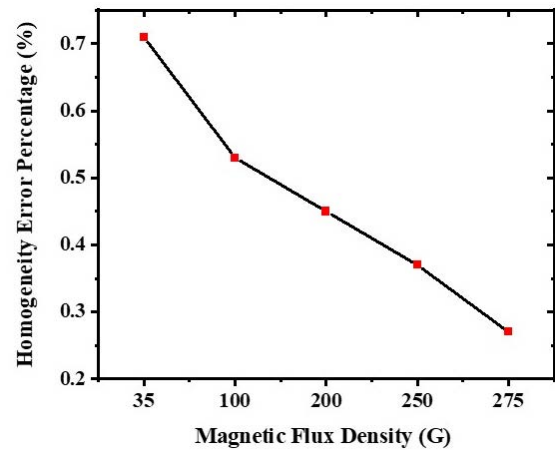

FIGURE 11. Magnetic field homogeneity error percentage.

the maximum flux density value, and the higher homogeneity error percentage value occurs at the lower flux density value. So, the overall homogeneity error percentage of the calibration device is lower than 1%. The reason for these minor errors is due to the variation of the probe adjusting gap.

TABLE 4. Measurement values of the magnetic flux density.

Current (Amp)	Theory (Gauss)	Simulation (Gauss)	Experiment (Gauss)
0.25	31.55	33.63	34.7
0.50	63.10	67.27	69.0
0.75	94.66	100.90	103.3
1.00	126.21	134.54	138.6
1.25	157.77	168.17	172.0
1.50	189.88	201.81	206.6
1.75	220.87	235.44	241.0
2.00	252.43	269.08	275.2

IV. DISCUSSIONS

The designing process of the stable homogeneous magnetic field calibration device illustration results from the theoretical, simulation, and experimental are mentioned in Table 4. The parameters mentioned in Table 1 are used to calculate and measure the present results. Those results are actual operating results. The magnetic flux density is obtained from 34.7 G to 275.2 G at the current intervals of I = 0.25 A to I = 2.0 A. In order to design a physical device, the magnetic flux density was examined earlier in two methods such as theoretical and simulation for proofreading. According to the theoretical results, the magnetic flux density was obtained from 31.55 G to 252.43 G. As per the simulation, and the magnetic flux density was obtained from 33.63 G to 269.08 G. The current value is used as an analog step of 0.25 A in a theoretical, simulation, and experimental. This current value is not fixed for the calculation and measurement. In theory, simulation, and experimental methods, it may also be measured in 0.1 A

or each 0.3 A. We observed that 0.25 A is the best in the theoretical method's steps.

TABLE 5. Error percentage (%) values.

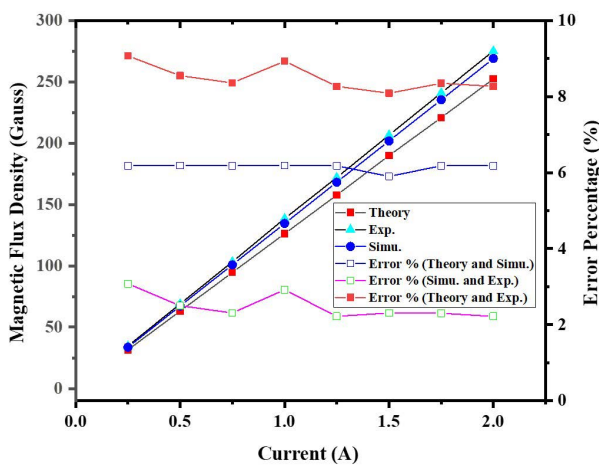| Theory and Simulation	Theory and Experiment	Simulation and Experiment
6.18	9.07	3.08
6.19	8.55	2.50
6.18	8.36	2.31
6.19	8.93	2.92
6.18	8.27	2.22
5.90	8.09	2.31
6.18	8.35	2.30
6.18	8.27	2.22

FIGURE 12. Magnetic flux density vs. current and error percentage vs. current, in theory, simulation, and experimental.

Table 5 shows the device's theory, simulation, and experimental error percentage values. The error percentage values were obtained by comparing the theoretical device values with the simulation values, the device theoretical values with the experimental values, and the device simulation values with the experimental values. If the error percentage of theory vs. simulation is within 10%, these device values are acceptable to make the prototype. However, if the error percentage is greater than 10%, these values are unacceptable. Therefore, return to the theoretical step and adjust the device parameters. In this case, the maximum error percentage is 6.19%, as shown in Table 5. Hence, these parameters are used to make the prototype of the calibration device. The obtained experimental measurement results are compared with the theoretical results, the maximum error percentage is 9.07%, as shown in Table 5, and also compared with the simulation results, the maximum error percentage is 3.08%, as shown in Table 5. If the experimental values error percentage exceeds 10% of the finite element method error percentage and theoretical error percentage values, then recheck the experimental

method's settings parameters. The prototype will be accepted if the experimental error percentage value is within 10% of the theoretical and simulation error percentage values. Fig. 12 shows a graphical view of the research work. The graphical view shows the magnetic flux density in theory, simulation, and experimental. It also shows the error percentage between the theory and simulation, simulation and experimental, and theory and experimental. The theoretical graph shows that the magnetic flux density rises from 31.55 G to 252.43 G at I = 0.25 A to I = 2.0 A. The simulation graph increases from 33.63 G to 269.08 G at current values. The simulation graph line slightly increases than the theoretical graph line. For example, an experimental graph varies from 34.7 G to 275.2 G. By observing the theoretical, simulation, and experimental graphical lines, an experimental graphical line increases more than other graphical lines. The difference in the three methods' results and linearity and homogeneity errors are due to the measuring limit of the coils, location accuracy of the hall probe, the characteristics of the tape used in coil winding, and tight winding turns of the coil [36].

Error lines maintain the approximately same level of straight lines. An error percentage between the simulation and experimental shows a small error percentage compared with the other two error percentage lines. The maximum error percentage is 3.08%, slightly higher than the other current interval's error percentage values. An error percentage between the theory and simulation shows a straight line. It is higher than the simulation and experimental error percentage graph line. However, the theory and experimental results show the maximum error percentage value of 9.07%. This is higher than the error percentage of theory and simulation. The straight line illustrates that strength increases from low current magnitude to high current magnitude. It shows high linearity and reliability, especially in simulation and experimental results.

V. CONCLUSION

This paper introduced the new design of the calibration device by using circular coils for a stable homogeneous magnetic field strength. The theoretical, simulation and experimental methods [37], [38], [39] have examined the coils' magnetic field strength. The theoretical value can be deduced before the actual prototype by the present research work's design method. Then, the re-calculating can be applied to the theoretical value method with the help of FEM simulation results. This is the verification method in our design, and also, there is an opportunity for the first error correction to produce results similar to the ideal values by using the revised parameters obtained from the FEM method manufactured a device prototype. However, with the help of these designing methods, reducing the possibility of wrong attempts can also significantly reduce the time for adjusting the product value deviation and maintaining the calibration device's stability. The present work also uses electromagnetic characteristics due to the parameters of the coils that can adopt a stable homogeneous magnetic field strength. Different currents were

applied to the coil setup in three designing methods, depicting an increase in magnetic flux density by increasing the current value. We have compared the results and calculated the error percentage. The theoretical and simulation values obtained a constant error percentage of 6.18%. The simulation and experimental error percentages are less than 3.08%, and the theory and experimental maximum error percentage is 9.07%. This device can produce a magnetic flux density from 34.7 G to 275.2 G. This design method is beneficial for designing a high stability and linearity magnetic field generating device.

REFERENCES

[1] Q. Cao, X. Han, and L. Li, "Configurations and control of magnetic fields for manipulating magnetic particles in microfluidic applications: Magnet systems and manipulation mechanisms," *Lab Chip*, vol. 14, no. 15, pp. 2762–2777, 2014.

[2] M. Reta-Hernández and G. G. Karady, "Attenuation of low frequency magnetic fields using active shielding," *Electr. Power Syst. Res.*, vol. 45, no. 1, pp. 57–63, Apr. 1998.

[3] S. M. Satav and V. Agarwal, "Design and development of a low-cost digital magnetic field meter with wide dynamic range for EMC precompliance measurements and other applications," *IEEE Trans. Instrum. Meas.*, vol. 58, no. 8, pp. 2837–2846, Aug. 2009.

[4] G. Go, H. Choi, S. Jeong, C. Lee, S. Y. Ko, J.-O. Park, and S. Park, "Electromagnetic navigation system using simple coil structure (4 coils) for 3-D locomotive microrobot," *IEEE Trans. Magn.*, vol. 51, no. 4, pp. 1–7, Apr. 2015.

[5] S. S. Syu, "Magnetic torquer sensor for steering system," U.S. Patent 9 829 400 B2, Aug. 3, 2017.

[6] M. Abdelrahman and S.-Y. Park, "Integrated attitude determination and control system via magnetic measurements and actuation," *Acta Astronaut.*, vol. 69, nos. 3–4, pp. 168–185, Aug. 2011.

[7] T. Inamori, N. Sako, and S. Nakasuka, "Compensation of time-variable magnetic moments for a precise attitude control in nano- and micro-satellite missions," *Adv. Space Res.*, vol. 48, no. 3, pp. 432–440, Aug. 2011.

[8] M. Lovera and A. Astolfi, "Spacecraft attitude control using magnetic actuators," *Automatica*, vol. 40, no. 8, pp. 1405–1414, Aug. 2004.

[9] C. A. Washburn, "A magnetic deflection up-date: Field equations, CRT geometry, the distortions and their corrections," *IEEE Trans. Consum. Electron.*, vol. 41, no. 4, pp. 963–978, Nov. 1995.

[10] K. H. Park, B. K. Kang, M. Yoon, and J. H. Lim, "Rotating coil method for the measurement of deflecting magnetic fields in cathode ray tube," *Sens. Actuators A, Phys.*, vol. 86, no. 3, pp. 159–164, Nov. 2000.

[11] K. H. Park, M. Yoon, D. E. Kim, S. M. Lee, H. D. Joo, S. D. Lee, and W. Y. Yang, "A three-dimensional magnetic field mapping system for deflection yoke of cathode-ray tube," *J. Inf. Display*, vol. 3, no. 4, pp. 19–22, Jan. 2002.

[12] A. F. R. Alvarez, E. F. Mejia, H. C. Ramirez, and C. R. Pinedo Jaramillo, "Analysis of the magnetic field homogeneity for an equilateral triangular Helmholtz coil," *Prog. Electromagn. Res. M*, vol. 50, pp. 75–83, 2016.

[13] A. F. Restrepo, E. Franco, H. Cadavid, and C. R. Pinedo, "A comparative study of the magnetic field homogeneity for circular, square and equilateral triangular Helmholtz coils," in *Proc. Int. Conf. Electr., Electron., Commun., Comput., Optim. Techn. (ICEECCOT)*, Dec. 2017, pp. 13–20.

[14] S. Chen, Y. Li, Y. Dai, Y. Lei, and L. Yan, "Quench protection design of a 9.4 T whole-body MRI superconducting magnet," *Phys. C, Supercond. Appl.*, vol. 497, pp. 49–53, Feb. 2014.

[15] D. Gurrera, K. K. Gallias, M. Spanà, B. F. Abbate, F. D'Alia, G. Iacoviello, and V. Caputo, "Moving across the static magnetic field of a 1.5 T MRI scanner: Analysing compliance with directive 2013/35/EU," *Phys. Medica*, vol. 57, pp. 238–244, Jan. 2019.

[16] C. R. Meixner, P. Liebig, P. Speier, C. Forman, B. Hensel, M. Schmidt, M. Saake, M. Uder, A. Doerfler, R. M. Heidemann, S. Schmitter, and A. M. Nagel, "High resolution time-of-flight MR-angiography at 7 T exploiting VERSE saturation, compressed sensing and segmentation," *Magn. Reson. Imag.*, vol. 63, pp. 193–204, Nov. 2019.

[17] E. Motovilova, S. Sandeep, M. Hashimoto, and S. Y. Huang, "Water-tunable highly sub-wavelength spiral resonator for magnetic field enhancement of MRI coils at 1.5 T," *IEEE Access*, vol. 7, pp. 90304–90315, 2019.

[18] S. S. Syu and G. K. Manchala, "A design method for a stable homogeneous magnetic field generating device," T.W. Patent I 725 872, Apr. 21, 2021.

[19] A. K. Boadi, H. Shimoji, T. Todaka, and M. Enokizono, "Designing of suitable construction of high-frequency induction coil by using finite element method," in *Proc. IEEE Int. Magn. Conf. (INTERMAG)*, vol. 41, Apr. 2005, pp. 1077–1078.

[20] G. Fois, A. Floris, A. Serpi, M. Porru, and A. Damiano, "Design criteria for ferrite-based high-speed permanent magnet synchronous machines," in *Proc. 7th Int. Electr. Drives Prod. Conf. (EDPC)*, Dec. 2017, pp. 1–7.

[21] M. Shadmand and R. Balog, "Determination of parasitic capacitances in high frequency coupled inductors filters using finite-element methods," Res. Gate, Tech. Rep., Sep. 2011, doi: 10.13140/RG.2.1.4773.5209.

[22] A. Saadha, C. V. Aravind, P. Krishna, and F. Azhar, "Design analysis of taper width variations in magnetless linear machine for traction applications," *J. Eng. Sci. Technol.*, vol. 13, pp. 17–26, Sep. 2018.

[23] A. Razali, F. Rahman, Y. W. Leong, M. R. Hanipah, and M. A. Hizami, "Performance and optimum characteristics by finite element analysis of a coreless ironless electric generator for low wind density power generation," *IOP Conf. Ser., Mater. Sci. Eng.*, vol. 342, no. 1, pp. 1–8, 2018.

[24] M. Jenal, E. Sulaiman, M. F. Omar, G. M. Romalan, and H. A. Soomro, "Development of a novel permanent magnet flux switching machine prototype for light weight electric vehicles," in *Proc. IEEE Student Conf. Res. Develop. (SCOReD)*, Dec. 2015, pp. 739–744.

[25] N. De Zanche, C. Barmet, J. A. Nordmeyer-Massner, and K. P. Pruessmann, "NMR probes for measuring magnetic fields and field dynamics in MR systems," *Magn. Reson. Med.*, vol. 60, no. 1, pp. 176–186, Jul. 2008.

[26] C. Schott, R. S. Popovic, S. Alberti, and M. Q. Tran, "High accuracy magnetic field measurements with a Hall probe," *Rev. Sci. Instrum.*, vol. 70, no. 6, pp. 2703–2707, Jun. 1999.

[27] J. Zhang, K. W. Kam, J. Min, V. V. Khilkevich, D. Pommerenke, and J. Fan, "An effective method of probe calibration in phase-resolved near-field scanning for EMI application," *IEEE Trans. Instrum. Meas.*, vol. 62, no. 3, pp. 648–658, Mar. 2013.

[28] S. Tumanski, *Handbook of Magnetic Measurements*, 1st ed. New York, NY, USA: CRC Press, 2011, p. 85.

[29] J. Parsa and M. Mohammadzadeh, "Design and fabrication of a new multi-loop saddle coil for 1.5 T MRI," *Rev. Sci. Instrum.*, vol. 90, no. 11, 2019, Art. no. 114707.

[30] A. Kageyama, T. Miyagoshi, and T. Sato, "Formation of current coils in geodynamo simulations," *Nature*, vol. 454, no. 7208, pp. 1106–1109, Aug. 2008.

[31] P. Blümler, "Proposal for a permanent magnet system with a constant gradient mechanically adjustable in direction and strength," *Concepts Magn. Reson. B, Magn. Reson. Eng.*, vol. 46, no. 1, pp. 41–48, 2016.

[32] R. Hurtado-Velasco and J. Gonzalez-Llorente, "Simulation of the magnetic field generated by square shape Helmholtz coils," *Appl. Math. Model.*, vol. 40, nos. 23–24, pp. 9835–9847, Dec. 2016.

[33] D.-S. Filip and D. Petreus, "Simulation of a four resonant coil power transfer system," in *Proc. Int. Conf. Optim. Electr. Electron. Equip. (OPTIM), Int. Aegean Conf. Electr. Mach. Power Electron. (ACEMP)*, May 2017, pp. 196–201.

[34] N. Sulaiman and B. Y. Majlis, "Simulation study of side-by-side spiral coil design for micromagnetometer," in *Advanced Materials Research*, vol. 254. Switzerland: Trans Tech Publications, 2011, pp. 175–178.

[35] W. T. B. DeSousa, A. Polasek, T. M. L. Assis, R. DeAndrade, and M. Noe, "Simulations of resistive and air coil SFCLs in a power grid," *IEEE Trans. Appl. Supercond.*, vol. 25, no. 3, pp. 1–5, Jun. 2015.

[36] A. Mochida, H. Ueda, S. Noguchi, T. Wang, A. Ishiyama, H. Miyazaki, T. Tosaka, S. Nomura, T. Kurusu, S. Urayama, and H. Fukuyama, "Evaluation of magnetic field distribution by screening current in multiple REBCO coils," *IEEE Trans. Appl. Supercond.*, vol. 26, no. 4, pp. 1–5, Jun. 2016.

[37] P. Baranov, V. Baranova, S. Uchaikin, and Y. Pisarenko, "Creating a uniform magnetic field using axial coils system for calibration of magnetometers," in *Proc. Dyn. Syst. Mech. Mach. (Dynamics)*, 2016, pp. 1–5.

[38] Z. Zhang, C. H. Kim, J. G. Kim, J. Kvitkovic, S. Pamidi, M. Zhang, J. Li, and W. Yuan, "An experimental investigation of the transient response of HTS non-insulation coil," *J. Supercond. Novel Magn.*, vol. 30, no. 2, pp. 387–393, Feb. 2017.

[39] M. S. Crosser, S. Scott, A. Clark, and P. M. Wilt, "On the magnetic field near the center of Helmholtz coils," *Rev. Sci. Instrum.*, vol. 81, no. 8, Aug. 2010, Art. no. 084701.

SHAO SYUAN SYU received the B.S. degree in electrical engineering from the National Chiayi University, Taiwan, in 2007, and the M.S. degree in electrical engineering from Tunghai University, Taichung, Taiwan, in 2009. He is currently pursuing the Ph.D. degree in materials science and engineering with the National Chung Hsing University, Taichung.

From 2010 to 2013, he worked as a RF IC Product Engineer at Sigurd Microelectronics Corporation, Taiwan. From 2014 to 2017, he served as a Project Manager for designing and developing the magnetic torque sensor for the automotive electronic power steering system at Rotatech Ltd., and he successfully finished that project. Since 2018, he has been served as the Product Manager for magnetic technology solutions and engaged in technical services with the Mobilsens Technologies, Taichung. In addition, he has focused on the five magnetic-related invention patents in the past few years. His research interests include the standard measurement and calibration of electromagnetic field systems, the manufacture, and application of soft magnetic alloys, the application of automatic magnetization systems, and the design and control of magnetic encoders.

Mr. Syu is a member of the U.K. Magnetics Society and the Taiwan Association for Magnetic Technology Member.

MANCHALA GOPALA KRISHNA was born in Guntur, Andhra Pradesh, India, in 1994. He received the B.Tech. degree in mechanical engineering from VFSTR University, Guntur, in 2016, and the M.S. degree in mechanical engineering from the Southern Taiwan University of Science and Technology, Tainan, Taiwan, in 2019. He is currently working as a Research and Development Engineer with the Mobilsens Technologies, Taichung, Taiwan. His research interest includes the design and development of electromagnetic devices.

ROSHNI YADAV (Graduate Student Member, IEEE) received the B.Tech. degree in electronics and communication engineering from BBDNIIT, and the M.Tech. degree in nano-optoelectronics from Babasaheb Bhimrao Ambedkar University (Central University), Lucknow, Uttar Pradesh, India. She is currently pursuing the Ph.D. degree with the National Chung Hsing University, Taiwan. Her research interests include magnetic materials and polarized neutron reflectometry (PNR).
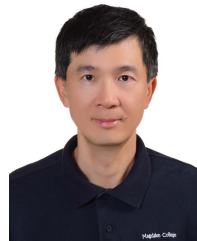
KO-WEI LIN (Senior Member, IEEE) received the B.S. degree from Feng Chia University, in 1992, the M.S. degree from the National Taiwan University, Taiwan, in 1994, and the Ph.D. degree from the State University of New York, Stony Brook, in 2002. He became a Postdoctoral Fellow at the Toyota Technological Institute, Japan. Since 2003, he has been as one of the Faculty Member with the Department of Materials Science and Engineering (MSE), National Chung Hsing University (NCHU), Taichung, Taiwan. His research interests include fabricating magnetic thin films by ion-beam techniques and characterization, including using polarized neutron reflectometry (PNR). He served as the Department Chair (2018–2020) of MSE, NCHU, and also the President of Taiwan Neutron Science Society (2018–2020). He is currently a Full Professor with MSE, NCHU; and the Taiwan Chapter Chair of IEEE Magnetics Society.

• • •